AFRL-RX-WP-TP-2011-4219

PRECIPITATION OF ORDERED PHASES IN METALLIC SOLID SOLUTIONS: A SYNERGISTIC CLUSTERING AND ORDERING PROCESS (PREPRINT)

R. Banerjee, A. Singh, and S. Nag

University of North Texas

G.B. Viswanathan and Jaimie Tiley

Metals Branch
Metals, Ceramics, and NDE Division

H.L. Fraser

The Ohio State University

JULY 2011

AIR FORCE RESEARCH LABORATORY
MATERIALS AND MANUFACTURING DIRECTORATE
WRIGHT-PATTERSON AIR FORCE BASE, OH 45433-7750
AIR FORCE MATERIEL COMMAND
UNITED STATES AIR FORCE

REPORT DOCUMENTATION PAGE

Form Approved
OMB No. 0704-0188

1. REPORT DATE *(DD-MM-YY)*	2. REPORT TYPE	3. DATES COVERED *(From - To)*
July 2011	Journal Article Preprint	01 July 2011 – 01 July 2011

4. TITLE AND SUBTITLE
PRECIPITATION OF ORDERED PHASES IN METALLIC SOLID SOLUTIONS: A SYNERGISTIC CLUSTERING AND ORDERING PROCESS (PREPRINT)

5a. CONTRACT NUMBER
FA8650-08-C-5226

5b. GRANT NUMBER

5c. PROGRAM ELEMENT NUMBER
62102F

6. AUTHOR(S)
R. Banerjee, A. Singh, and S. Nag (University of North Texas)
G.B. Viswanathan and Jaimie Tiley (AFRL/RXLM)
H.L. Fraser (The Ohio State University)

5d. PROJECT NUMBER
4349

5e. TASK NUMBER
00

5f. WORK UNIT NUMBER
LM114100

7. PERFORMING ORGANIZATION NAME(S) AND ADDRESS(ES)
University of North Texas
Denton, TX 76203

The Ohio State University
Columbus, OH 43210

Metals Branch (AFRL/RXLM)
Metals, Ceramics, and NDE Division
Air Force Research Laboratory
Materials and Manufacturing Directorate
Wright-Patterson Air Force Base, OH 45433-7750
Air Force Materiel Command, United States Air Force

8. PERFORMING ORGANIZATION REPORT NUMBER

9. SPONSORING/MONITORING AGENCY NAME(S) AND ADDRESS(ES)
Air Force Research Laboratory
Materials and Manufacturing Directorate
Wright-Patterson Air Force Base, OH 45433-7750
Air Force Materiel Command
United States Air Force

10. SPONSORING/MONITORING AGENCY ACRONYM(S)
AFRL/RXLM

11. SPONSORING/MONITORING AGENCY REPORT NUMBER(S)
AFRL-RX-WP-TP-2011-4219

12. DISTRIBUTION/AVAILABILITY STATEMENT
Approved for public release; distribution unlimited.

13. SUPPLEMENTARY NOTES
PAO Case Number: 88ABW 2011-1189; Clearance Date: 09 Mar 2011. Document contains color.
Journal article submitted from publication in *Physics Review Letters*.

14. ABSTRACT
The precipitation mechanism of ordered phases in metallic solid solutions has been a long-standing controversy due to the competing roles of chemical clustering (or phase separation) and chemical ordering. In the present study, this controversy has been resolved through the coupled use of aberration-corrected high-resolution scanning transmission electron microscopy and atom probe tomography. Thus, the experimental results, obtained at atomic resolution, can be interpreted satisfactorily only on the basis of phase separation via spinodal decomposition followed by chemical ordering.

15. SUBJECT TERMS
precipitation mechanism, metallic solid solutions, chemical clustering, chemical ordering

16. SECURITY CLASSIFICATION OF:			17. LIMITATION OF ABSTRACT:	18. NUMBER OF PAGES	19a. NAME OF RESPONSIBLE PERSON (Monitor)
a. REPORT	b. ABSTRACT	c. THIS PAGE			Jaimie Tiley
Unclassified	Unclassified	Unclassified	SAR	24	19b. TELEPHONE NUMBER *(Include Area Code)* N/A

Precipitation of Ordered Phases in Metallic Solid Solutions: A Synergistic Clustering and Ordering Process

G. B. Viswanathan[1], R. Banerjee[2], A. Singh[2], S. Nag[2], J. Tiley[1], and, H. L. Fraser[3]

[1]Materials and Manufacturing Directorate, Air Force Research Laboratory, Dayton, Ohio 45309, U. S. A.

[2]Center for Advanced Research and Technology, Department of Materials Science and Engineering, University of North Texas, Denton, Texas 76203, U. S. A.

[3]Center for the Accelerated Maturation of Materials, Department of Materials Science and Engineering, The Ohio State University, Columbus, Ohio 43210, U. S. A.

Abstract

The precipitation mechanism of ordered phases in metallic solid solutions has been a long-standing controversy due to the competing roles of chemical clustering (or phase separation) and chemical ordering. In the present study, this controversy has been resolved through the coupled use of aberration-corrected high-resolution scanning transmission electron microscopy and atom probe tomography. Thus, the experimental results, obtained at atomic resolution, can only be interpreted satisfactorily on the basis of phase separation via spinodal decomposition followed by chemical ordering.

Introduction

Concurrent chemical clustering and ordering processes occurring within the same supersaturated solid solution comprise an interesting class of solid-solid phase transformations that can often lead to a homogeneous distribution of nanoscale ordered precipitates within a disordered solid solution matrix [1-3] often resulting in enhanced mechanical properties such as high temperature strength. Typically, these two processes are considered mutually exclusive since chemical clustering involves a preference

towards formation of bonds between like atoms, leading to compositional partitioning within the metallic solid solution, while ordering involves a preference towards the formation of bonds between unlike atoms leading to an ordered structure. When a disordered solid solution is rapidly cooled (or quenched) from a single phase field to a temperature corresponding to a two-phase field, the resulting highly undercooled and supersaturated disordered solid solution is often unstable (or metastable) with respect to both clustering and ordering processes [3]. There are a number of examples in the literature that discuss the possibility of such concurrent clustering and ordering processes in metallic solid solutions including Fe-Al [4], Ni-Al [5,6], Ni-Ti [7,8], and Cu-Ti [9,10]. While the order-disorder reaction in Fe-Al is a second (or higher) order reaction, in case of Ni-Al and Ni-Ti alloys the ordering involves a first-order reaction. Furthermore, there has been a substantial amount of controversy in the literature regarding whether the spinodal clustering (or phase separation) precedes or is subsequent to the ordering reaction. In most cases, reports indicate that the chemical ordering precedes the spinodal decomposition since the ordering process involves short-range atomic jumps which are relatively easy to accomplish and hence take place faster compared with the longer range diffusion required for spinodal decomposition [1-3,11]. A few exceptions to this include the reports in Ni-Ti [6,7] and more recently in the Cu-Ni-Sn [11] systems, where spinodal decomposition has not only been reported to precede but also has been a prerequisite for the ordering reaction to take place. The proposition is that since the Cu-15Ni-8Sn alloy composition cannot undergo congruent ordering, spinodal decomposition creates Sn-rich domains within which DO_{22} (and subsequently $L1_2$) ordering can take place [12]. Despite these interesting experimental observations, in almost all these cases the evidence

indicating concurrent spinodal decomposition and ordering is based primarily on diffraction (electron or x-ray) data as well as diffraction contrast images recorded in a transmission electron microscope. Direct observation of the early stages of concurrent (or sequential) spinodal decomposition and ordering processes is simply not possible using these particular techniques. Recent developments in aberration-corrected scanning transmission electron microscopy (STEM) and complementary technique such as atom probe tomography (APT) now permit the visualization of these complex solid-state transformations at their very early stage. Therefore, this letter focuses on capturing and directly imaging these complementary processes of spinodal decomposition and chemical ordering at atomic resolution as well as measuring the resultant compositional partitioning at very early stages of the transformation.

In the case of formation of the γ', Ni_3Al-based ($L1_2$ ordered), phase within the disordered face-centered cubic (fcc) γ solid-solution matrix of Ni-base alloys containing Al and other alloying additions, there has been some controversy in the literature regarding the precipitation mechanism. Thus, while a number of reports clearly classify γ' precipitation in the γ matrix as a classical nucleation and growth process [12,13], there are others which have claimed spinodal behavior [14,15]. For example, Hill and Ralph [14] suggested that the precipitation process may involve spinodal decomposition, based on results of atom probe field-ion microscopy (APFIM) studies of Ni-Al alloys. Interestingly, there are issues regarding this interpretation of their results. For example, Wendt and Hassan noted from [14] that in samples of the quenched alloy that have been briefly aged (30 minutes at 898K) the composition of the Al-rich regions (~5 nm) was

Ni-25at%Al, i.e. the stoichiometric γ' composition, implying that the phase separation was complete. Actually, it was reported in [14] that the composition of Al-rich regions in the *as-quenched* alloy also corresponds to stoichiometry. Based on this argument, it was claimed [13] that the precipitation process involved a classical nucleation and growth mechanism. Because of these conflicting views, it is clear that the γ' precipitation mechanisms are not known. This letter reports novel results which permit identification of these mechanisms of γ' precipitation in highly undercooled samples of a Ni-base superalloy by coupling aberration-corrected STEM with APT investigations.

Experiments were carried out on the commercial Ni base superalloy alloy, Rene'88 DT-56.53Ni-16.24Cr-13.27Co-3.92Ti-2.09Al-4.08Mo-3.92W-0.76Nb (in wt%) or 55.63Ni-18.02Cr-13.00Co-4.74Ti-4.45Al-2.48Mo-1.21W-0.46Nb (at%) [16]. In order to obtain the highest possible cooling rates, thin sections of the alloy (< 2mm) were solution treated in the single γ phase-field at 1150°C for 60 minutes in vacuum followed by a very rapid quench in ice-water that was kept in an inert Ar atmosphere. The purpose of the very rapid quench was to arrest or capture the formation of the ordered γ′ precipitates at the earliest stage. Samples for transmission electron microcopy (TEM) studies were prepared by extracting a thin foil by the focused ion beam method (FIB), followed by low energy Ar ion milling on Fischione Model 1040 nano-mill system. Atomic resolution, Z(atomic mass)-contrast imaging was carried out in the High Angle Annular Dark Field (HAADF)-STEM mode on an FEI Titan 80–300 kV microscope, operated at 300 kV, equipped with a CEOS probe aberration corrector. Nanometer-scale compositional analysis of the same samples was carried out using APT in a local electrode atom probe

system (Cameca's LEAP™). Samples for atom probe analysis were prepared in a dual-beam FIB as per details discussed elsewhere [17]. All atom probe experiments were carried out in the laser pulse evaporation mode at a temperature of 50K using a pulse energy of 0.2 nJ and a pulse frequency of 200 KHz.

Fig. 1(a) shows a selected area electron diffraction pattern from the as-quenched Rene 88DT Ni-base superalloy sample recorded along the [001] zone axis of the *fcc* γ matrix. In addition to the fundamental {200} and {220} reflections (or intensity maxima) from the *fcc* γ matrix, there are additional weak superlattice reflections clearly visible at the {100} and {110} locations, indicating the presence of $L1_2$ ordering within the γ matrix. Additionally, satellite reflections are present near the fundamental matrix reflections. Two such reflections have been marked in Fig. 1(a) and their presence is indicative of phase separation (or compositional clustering) consistent with previous observations of spinodal decomposition [11,18]. Hence, these satellite reflections have been labeled "spinodal" in the diffraction pattern. These satellite intensity maxima correspond to a modulation wavelength of ~ 2 nm. The collective diffraction evidence (i.e., superlattice and satellite reflections) is consistent with the co-existence of spinodal decomposition and chemical ordering within the *fcc* matrix.

High-resolution Z-contrast imaging, carried out in HAADF-STEM mode in an aberration-corrected electron microscope, revealed atomic scale information regarding the nature of these ordered regions as shown in Figs. 1(b) and (c). While Fig. 1(b) shows the raw HAADF-STEM image recorded with the electron beam parallel to the [011] zone

axis of the γ matrix, Fig. 1(c) shows the filtered (i.e., background-subtracted) image which provides for improved contrast and enhanced image clarity. A lower magnification HAADF-STEM has also been included as an inset in Fig. 1(c). The contrast visible in these HAADF-STEM can be correlated directly to Z-contrast or atomic mass contrast, where brighter regions have a higher concentration of heavier solute elements (e.g. Co, Cr, W, Nb) while regions of darker contrast are likely to contain higher concentrations of lighter elements (e.g. Al, Ti). The contrast between these brighter and darker regions within the γ matrix is more clearly visible in the lower magnification image shown as an inset in Fig. 1(c). Interestingly, these regions of brighter and darker contrast, visible in the HAADF-STEM images appear to be interconnected, a feature characteristic of a spinodally-decomposed microstructure [19].

Similar conclusions can be drawn for the differences in contrast between individual atomic columns in these HAADF-STEM images, with the brighter columns belonging to the Ni sublattice in the Ni_3Al-based $L1_2$ ordered structure, while the darker atomic columns belong to the Al sublattice. Nanometer-scale regions exhibiting a relatively darker contrast are marked with circles in Figs. 1(b) and (c). Closer inspection of these regions shows the presence of an ordered structure within these regions with rows of brighter atomic columns (Ni sublattice) alternating with rows containing 50% brighter (Ni sublattice) and 50% darker (Al sublattice) atomic columns. This pattern is consistent with an $L1_2$ ordered structure viewed along the [011] axis. $L1_2$ ordering is also confirmed by the presence of {100} and {110} spatial frequencies in the Fourier transform of the HAADF-STEM image shown as an inset in Fig. 1(b). Based on the HAADF-HRSTEM

analysis, the ordered domains nominally lie in the size range of 3 – 6 nm. In contrast, the nanometer-scale brighter regions in the HAADF-STEM images shown in Figs. 1(b) and (c), do not appear to exhibit the periodic arrangement of brighter and darker atomic columns, but rather all the atomic columns within the brighter regions appear to be nominally of the same contrast indicating a random solid solution. A more detailed analysis of the ordering and disordering in various regions will be presented subsequently in this letter (refer to the discussion of Fig. 3).

A section of a 3D tomographical reconstruction (70 nm x 70 nm x 180 nm) of the atom probe data recorded from the rapidly cooled sample is shown in Fig. 2(a). Since previous studies on the same Ni base superalloy [20] indicate that Cr is the most strongly partitioning element between the γ and γ' phases in this alloy, the Cr-rich and Cr-depleted regions have been clearly delineated by plotting a Cr=18at% iso-concentration surface (or isosurface) in Fig. 2(a). Thus, the regions within this Cr isosurface (encompassed by concave interfaces) contain less than 18%Cr while the regions outside the isosurface contain higher amounts of Cr. This 3D reconstruction reveals several interesting aspects of the microstructure. Firstly, despite the rapid quench rate experienced by this sample, there is significant partitioning of Cr at the nanoscale. Secondly, the Cr-enriched and Cr-depleted regions are interconnected as would be expected in case of a spinodally decomposed microstructure.

Fig. 2(b) shows a proximity histogram analysis for the Cr=18at% isosurface shown in Fig. 2(a). Composition profiles for the primary solute elements in this Ni-base alloy, Cr,

Co, Ti, Al, and Mo, across the interface defined by the isosurface, have been plotted in this figure. While there is partitioning of the solute elements across the interface, the compositional gradient is rather diffuse for all these elements with an interface width ~ 4 nm (for Cr, Ti, and Al). Such a diffuse compositional gradient is consistent with the early stages of a spinodally-decomposed microstructure with compositional modulations of small amplitude present throughout the matrix [19] leading to local nanometer scale domains enriched in Al and Ti while being depleted in Co, Cr, and Mo. Based on the HAADF-STEM images (Fig. 1) it appears that the $L1_2$ ordered domains are discrete and lie in the size range of 3–6 nm. Therefore, the Cr=18at% isosurface, exhibiting an interconnected network, possibly does not delineate the γ' domains. Previous results indicate that the γ' phase can be best delineated using a Cr=14at% isosurface for this alloy [20, 21]. Using a similar analogy in the present study, constructing a Cr=14at% isosurface (Fig. 2(c)) results in Cr-depleted domains in the range of 3-8 nm, which is in good agreement with the HAADF-STEM results (Fig. 1(b) and (c)). The average composition of these Cr-depleted ordered regions was determined to be Ni-9.1Co-6.9Cr-8.5Al-9.4Ti-2.7Mo (all in at%). The composition of these ordered domains is substantially different from the near-equilibrium composition of larger γ' precipitates (Ni-6.5Co-1.7Cr-12.3Al-9.2Ti-2.9Mo, all in at%) reported in previous atom probe studies of the same alloy after long-term aging at 760°C [21]. The substantially higher concentration of Co and Cr and a lower concentration of Al within the γ' precipitates in the rapidly quenched alloy are indicative of ordering taking place at far-from equilibrium compositions.

A more detailed analysis of the ordered and disordered structures present within different regions of the fcc γ matrix has been presented in the HAADF-STEM images shown in Fig. 3. Three different nanoscale regions of the matrix, exhibiting two different levels of contrast (different average atomic masses) are shown in this figure. The regions exhibiting the lighter contrast (e.g., Fig. 3(a)) are always disordered. The regions exhibiting the darker contrast are sometimes ordered (e.g., Fig. 3(b)) and sometimes disordered (e.g., Fig. 3(c)). **[Change Fig Seq]** The corresponding intensity profiles, plotted along the <111> fcc direction (marked with a line in each figure) for each of these regions is shown in Fig. 3(d), confirming the ordered and disordered regions. These observations as well as other similar analyses carried out on different regions of the fcc matrix are indicative of a particular transformation sequence. The two possible transformation sequences are, congruent ordering within the entire matrix followed by phase separation (via spinodal decomposition) and subsequent disordering, or, phase separation followed by ordering. In terms of contrast levels, the former sequence would result in all regions exhibiting dark contrast being ordered. In contrast, the latter sequence would result in some regions exhibiting dark contrast being ordered (complete transformation sequence) while other dark regions are disordered (incomplete sequence), as observed in the present case.

The experimental observations presented in this letter can only be interpreted via a γ' precipitation mechanism involving a phase separation (via spinodal decomposition), creating nanoscale domains depleted in certain solute elements (e.g. Co, Cr, and Mo) while being enriched in other solute elements (e.g. Al and Ti) within the fcc γ matrix,

which subsequently undergo an $L1_2$ ordering reaction to form nanoscale γ' precipitates. This mechanism can be simply illustrated based on schematic Gibbs free energy (G) – composition (X_{Al}) plots of the γ and γ' phases, at a low temperature (highly undercooled into the γ+γ' phase field) where a miscibility gap arises for the fcc γ phase, as shown in Fig. 4. Since the average composition of the Ni-base alloy (X_0) lies within the spinodal region of the γ miscibility gap, the γ phase is unstable with respect to compositional fluctuations leading to continuous phase separation. This leads to solute (Al) lean and solute-enriched domains within the matrix. The continually increasing amplitude and wavelength of the compositional modulations eventually lead to the solute-rich domains crossing the $X(T_0)$ point, providing a driving force for $L1_2$ ordering and the formation of nanoscale γ' precipitates. However, this ordering takes place at a composition far-from equilibrium as observed experimentally. Subsequent isothermal annealing is expected to increase the solute partitioning driving the composition of the γ' precipitates towards equilibrium.

Summarizing, this letter presents, for the first time, atomic resolution evidence of synergistic spinodal decomposition and chemical ordering within a metallic solid solution. The specific example of a Ni-base superalloy highlights the important role played by prior phase separation within the fcc γ solid solution matrix resulting in appropriate nanoscale compositional domains within which ordering can take place.

References:

[1] W. A. Soffa and D. E. Laughlin, Proc. Int. Conf. Solid-Solid Transformations, ed. H. I. Aaronson, D. E. Laughlin, R. F. Sekerka and C. M. Wayman, TSM, Warrendale, Pennsylvania, 159 (1982)

[2] D. E. Laughlin and W. A. Soffa , Physical Properties and Thermodynamic Behavior of Minerals, NATO ASI Series C, Vol. 255, ed. E. K. H. Salje, D. Reidel, Dordrecht, 213 (1988)

[3] W. A. Soffa and D. E. Laughlin, Acta Metallurigica, 37, 3019 (1989)

[4] S. Allen and J. W. Cahn, Acta Metallurgica, 24, 425 (1976)

[5] W. O. Gentry and M. E. Fine, Acta Metallurgica, 20, 181 (1972)

[6] C. L. Corey, B. Z. Rosenblum and G. M. Greene, Acta Metallurgica, 21, 837 (1973)

[7] K. Saito and R. Watanabe, Japan J. Appl. Phys, 8, 14 (1969)

[8] R. Sinclair, J.A. Leake ad B. Ralph, Physica status solidi, 264, 285 (1974)

[9] D. E. Laughlin and J. W. Cahn, Acta Metallurgica, 329, (1975)

[10] D. E. Laughlin and J. W. Cahn, Met Trans, 5, (1974)

[11] J. –C. Zhao and M. R. Notis, Acta Materialia, 46, 4203 (1998)

[12] A. J. Ardell and R. B. Nicholson, Acta Metallurgica, 14, 1295 (1967).

[13] H. Wendt and P. Haasen, Acta Metallurgica, 31, 1649 (1983)

[14] S. A. Hill and B. Ralph, Acta Metallurgica, 30, 2219 (1982)

[15] W.O. Gentry and M.E. Fine, Acta Metallurgica, 20, 181 (1972)

[16] S. T. Wlodek, M. Kelly, D. A. Alden (1996) In: R. D. Kissinger, D. J. Deye, D. L. Anton, A. D. Cetel, M. V. Nathal, T. M. Pollock, D. A. Woodford (ed) Superalloys 1996, TMS, Warrendale, PA

[17] K. Thompson, D. Lawrence, D. J. Larson, J. D. Olson, T. F. Kelly, and, B. Gorman, *Ultramicroscopy*, , 107, 131 (2007)

[18] D. E. Laughlin, Acta Metallurgica, 24, 53 (1976)

[19] J. W. Cahn, Acta Metallurgica, 9 (1961).

[20] J. Y. Hwang, R. Banerjee , J. Tiley, R. Srinivasan, G. B. Viswanathan, H. L. Fraser, Metall. Mater. Trans. A 40:24 (2009).

[21] J. Y. Hwang, S. Nag, A. R. P. Singh, R. Srinivasan, J. Tiley, G. B. Viswanathan, H. L. Fraser, and R. Banerjee , Metall. Mater. Trans. A 40:3059 (2009).

Figure Captions:

Figure 1. (a) Selected Area Diffraction pattern of along the <001> fcc γ zone axis showing superalattice reflection of γ' and satellite spots. (b) HAADF-STEM image showing phase separated regions of darker and brighter contrast and ordering within the darker regions (Fourier transform of HAADF-STEM image shown as an inset). (c) Filtered (background-subtracted) HAADF STEM image (a low magnification HAADF-STEM image is shown as an inset).

Figure 2. Atom probe tomography results showing (a) 3D reconstruction of 18 at% Cr iso-concentration surface delineating Cr-rich and Cr-depleted regions as an interconnected network. (b) Proximity histogram corresponding to the 18at% Cr isosurface. (c) 14 at% Cr isosurface reconstruction with Ni ions.

Figure 3. High magnification HAADF-STEM images of (a) Dark ordered region (b)

Bright disordered region (c) Intermediate disordered region. (d) Intensity profiles along <111> direction in the corresponding dark-ordered, bright disordered and dark disordered regions.

Figure 4. Schematic G-X plots for both disordered γ and ordered γ’ phases showing the transformation pathway comprising spinodal decomposition followed by ordering.

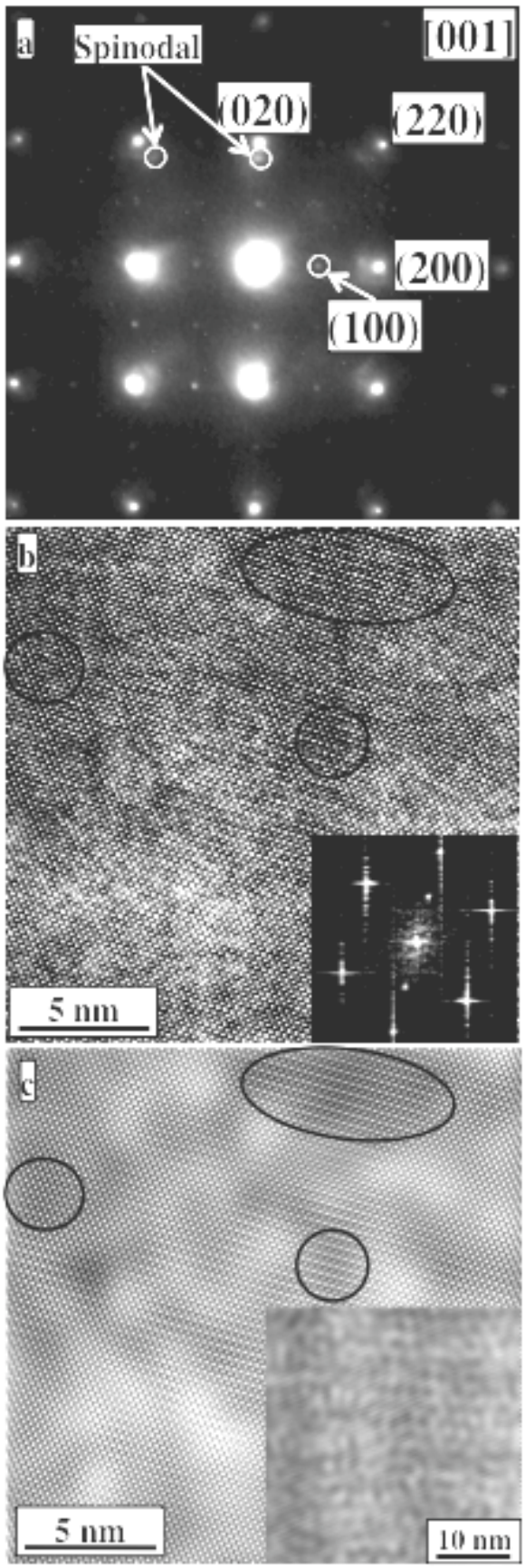

Fig. 1.

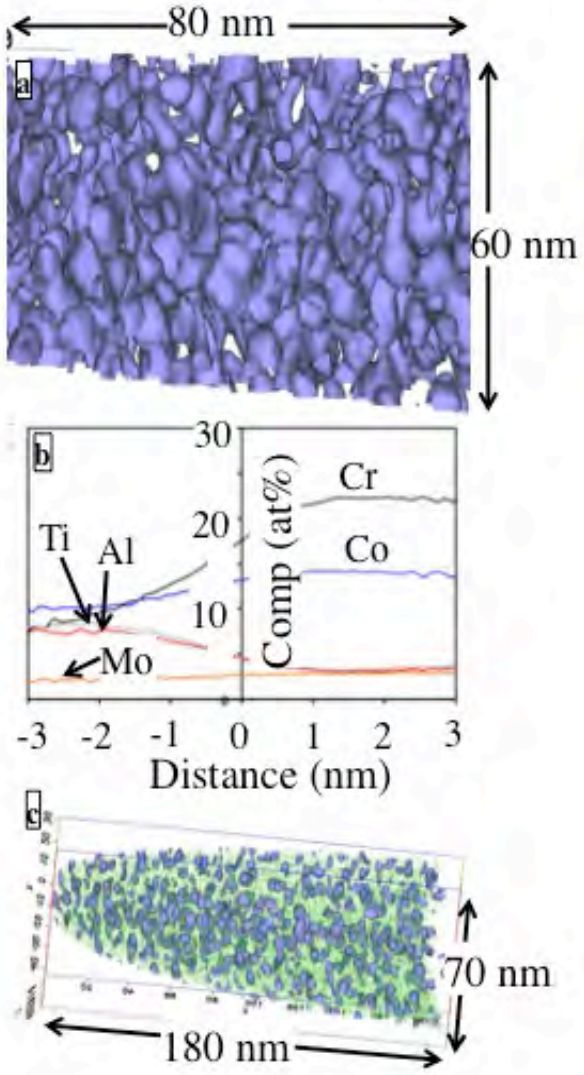

Fig. 2.

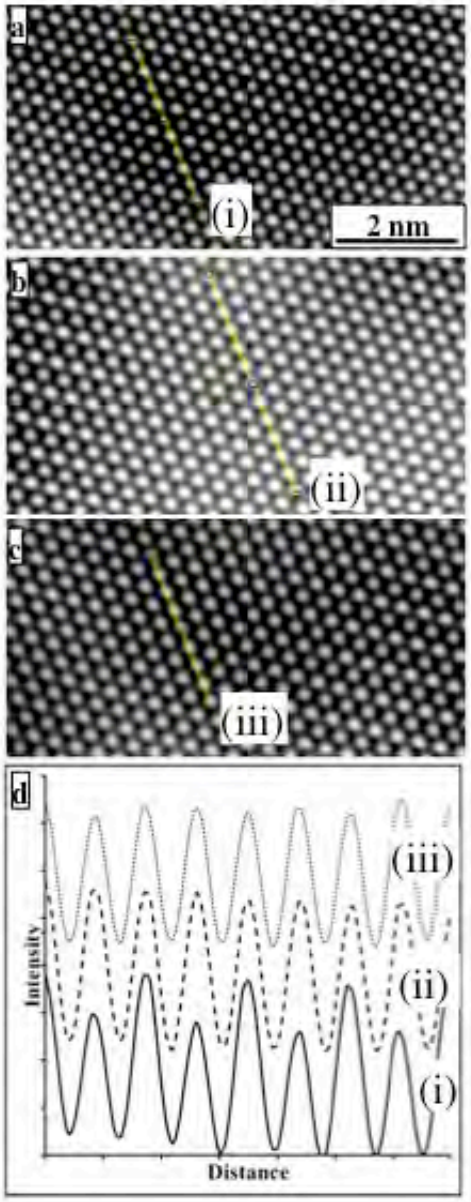

Fig. 3.

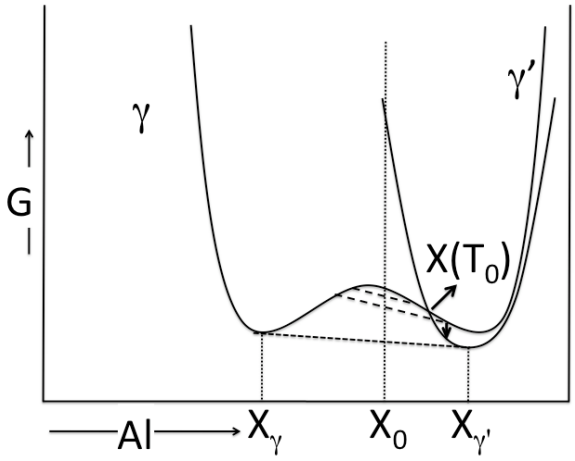

Fig. 4.